Electrically stimulated gradients in water and counterion concentrations within electroactive polymer actuators

Jong Keun Park,[a] Paul J. Jones,[b] Chris Sahagun,[b] Kirt A. Page,[c] Daniel S. Hussey,[d] David L. Jacobson,[d] Sarah E. Morgan[b] and Robert B. Moore*[a]

Received 3rd November 2009, Accepted 4th January 2010
First published as an Advance Article on the web 1st February 2010
DOI: 10.1039/b922828d

While ionic polymer metal composites (IPMCs) have been studied for more than 10 years, the specific actuation mechanism is still unclear. In this work, neutron imaging, applied potential atomic force microscopy (APAFM) and current sensing atomic force microscopy (CSAFM) methods are employed to fundamentally investigate the actuation mechanism of this electroactive polymer system. Direct neutron imaging allowed a mapping of the water–counterion concentration gradient profile (*i.e.*, a non-flat optical density profile sloping from the cathode to the anode) across an IPMC cross-section. While the neutron imaging method was capable of visualizing inside an operating IPMC, APAFM–CSAFM characterized changes in the nanoscale morphology and local surface properties due to redistribution of water–counterions under electrical stimulation. In APAFM, the darker, more energy dissipative features disappeared as the applied bias was varied from 0 V to 3 V, indicating that the surface became dehydrated. Surface dehydration undoubtedly supports the concept of proton and water migration to the negatively charged substrate. Water–counterion redistribution was further evidenced by CSAFM. With a negatively charged substrate (a 2 V bias), 2.8 pA of the average current were detected over the perfluorosulfonate ionomer (PFSI) surface in contact with AFM tip, which suggests the depletion of positively charged cations on the surface. On the contrary, a positively charged substrate (a −2 V bias) led to the average current of −90 pA over the PFSI surface in contact with the AFM tip, which indicates the formation of a cation-rich fluid on the top surface of the PFSI membranes. The observed water–counterion redistribution upon electrical stimulation directly supports a hydraulic contribution to the overall mechanism of actuation in IPMCs.

1. Introduction

Ionic polymer metal composites (IPMCs) are a class of stimuli-responsive materials that exhibit actuation with similarities to biological muscles, and are often referred to as artificial muscles.[1–9] IPMCs were first demonstrated in the early 1990's by Shahinpoor,[7] Sadeghipour[8] and Oguro *et al.*[9] IPMCs are based on a solid polymer electrolyte which is plated on both surfaces by metal nanoparticles (*e.g.*, platinum or gold) to serve as conductive electrodes. Under the stimulus of a relatively low electric field, IPMCs are capable of undergoing significant mechanical bending motion, while an external mechanical force applied to the surface of an IPMC can stimulate a detectable electrical response.[4]

A review of the open literature reveals that the perfluorosulfonate ionomer (PFSI) Nafion®[10] remains the benchmark material for the vast majority of IPMC research and technology development.[1,2] Nafion®, having a chemical structure shown in Fig. 1, is a copolymer of tetrafluoroethylene and generally less than 15 mol% of perfluorovinylether units terminated with sulfonic acid functionalities.[11] Great attention has been given to the unique nanophase-separated morphology observed upon aggregation of the polar, ionic moieties within the matrix of hydrophobic PTFE. The shape, spatial distribution and connectivity of polar ionic domains that are hydrophilic in nature precisely define the supramolecular organization. Numerous investigations have been focused on small angle X-ray and neutron scattering to propose detailed models for this technologically important material as an ionic conductor. While it is beyond the scope of this study to discuss all the models in detail, and the studies of Nafion® morphology remain inconclusive, it is generally accepted that there are continuous pathways that allow transport of ions and water[11–13] and recent studies have suggested elongated, locally parallel water channels.[12,14]

[a]*The Macromolecules and Interfaces Institute, Department of Chemistry, Virginia Polytechnic Institute and State University, Blacksburg, VA, USA. E-mail: rbmoore3@vt.edu*
[b]*School of Polymers and High Performance Materials, The University of Southern Mississippi, Hattiesburg, MS, USA*
[c]*Polymers Division, National Institute of Standards and Technology, Gaithersburg, MD, USA*
[d]*NIST Center for Neutron Research, National Institute of Standards and Technology, Gaithersburg, MD, USA*

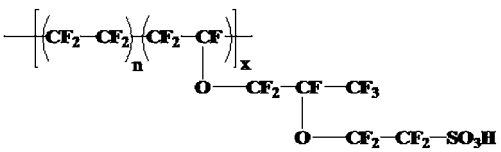

Fig. 1 Chemical structure of Nafion®.

While IPMCs have received extensive attention for more than 10 years and have been well explored with regard to nature and type of solvent,[15] electrode,[16,17] counterions,[18–20] and polymer electrolyte,[1–3,19,21] fundamental research to understand the specific underlying actuation mechanism is lacking. Upon electrical stimulation, the IPMC typically undergoes an initial rapid bending movement toward the anode. During application of a constant voltage, however, the IPMC is often observed to slowly relax in the opposite direction. One proposed mechanism for IPMC actuation has commonly been discussed in terms of electrophoresis-like counterion and water redistribution within the nanostructured ionomer membrane.[6,22,23] Since the ionic polymer is negatively charged with typically protons or alkali-metal cations as the counterions, these mobile cations in the hydrated membrane are readily redistributed in response to the applied electric field to create cation-rich and cation-poor boundary layers near the electrode–membrane interfacial regions. As cations migrate toward the cathode, they are accompanied by water molecules (*i.e.*, a hydraulic mechanism), which consequently causes swelling near the cathode and contraction (due to dehydration) near the anode. This swelling/contraction thus induces a bending force that curves the IPMC toward the anode. In contrast to a hydraulic model, which attributes actuation to charge and solvent transport, electrostatic models are based on a redistribution of cations and anions both within and at the surface of ionic aggregates.[24] According to the electrostatic model by Nemat-Nasser and Li,[25] fast bending actuation originates from local cation redistribution upon application of an electric field. The migration of cations results in relaxation of polymer chains in the anion-rich region and extension of polymer chains in the cation-rich region. Weiland and Leo proposed a slightly modified electrostatic actuation mechanism.[24] In contrast to the work of Nemat-Nasser and Li, Weiland and Leo propose that the initial rapid actuation behavior is dominated by a polarization mechanism, leaving only the slow relaxation to result from liquid and ion transport processes. The forces acting on dipoles located at the aggregate surface include dipole–dipole interactions, pendant chain stiffness, cluster surface energy and externally applied forces. Application of an external electric field is believed to cause the dipoles, that are assumed to have an equal magnitude and metastable orientations (all dipoles directed toward the center of the spherical cluster), to undergo reorientation and elongate or contract depending on their initial directions relative to the applied electric field. Macroscopic IPMC strain is then inferred from the distortion of the initially spherical aggregate into an ellipsoidal shape. The proposed model, however, relies on a number of simplifying assumptions which include very close contact between cation and anion in the hydrated state and primarily a spherical aggregate geometry not in tune with current Nafion® morphological models.[12,13]

In our recent investigation, the importance of the ionomer membrane morphology and chain conformation in the overall actuation phenomenon was clearly demonstrated for the first time.[2] Before full utilization of this unique electroactive material, a precise molecular-level understanding of the actuation mechanism is a prerequisite. Previous efforts to characterize water redistribution within IPMC include MRI[26] and NMR[27] methods, which showed greater proton density (PD) and higher water diffusion coefficients near the cathode, respectively. The current study involves an alternative, novel characterization approach that provides more direct evidence of the water–counterion redistribution under electrical stimulation. In this research, neutron imaging and atomic force microscopy techniques are employed. Since the IPMC materials explored consist of Nafion® membranes and Pt electrode layers, these samples are essentially equivalent to the chemical composition of fuel cell membrane electrode assembly (MEA) for which neutron imaging has proven to be of profound importance.[28–30] While the neutron imaging technique allows for direct imaging of electrically induced water–counterion concentration profiles across the IPMC cross-section with a spatial resolution of 25 μm, AFM studies provide characterization of water–counterion transport and monitoring of changes in the morphological and surface characteristics that result from electrical stimulation. With the aid of these complimentary techniques, we have obtained direct experimental evidence supporting long-range water–counterion redistribution during electrical stimulation.

2. Experimental

2.1 Materials

The perfluorosulfonate ionomer, Nafion® 117CS membranes (1100 g per equivalent, 7 mil thickness), were purchased from E.I. Dupont de Nemours & Co. and cleaned by refluxing in 8 M aqueous nitric acid for 2 h, and then in deionized (DI) water for 1 h.

2.2 Sample preparation for neutron imaging

Tetrabutylammonium (TBA^+) neutralized membranes were prepared by soaking the previously cleaned H^+-form membranes in 1 M tetrabutylammonium hydroxide (TBAOH) (Aldrich) in methanol solutions for 12 h and then rinsing with methanol to remove the residual TBAOH. TBA^+ neutralized membranes were dissolved in an alcohol–water mixture composed of the following volume fractions [methanol 30%, isopropanol 30%, and DI water 40%] under high temperature (*ca.* 250 °C) and high pressure (*ca.* 7000 kPa) conditions.[31] The solution was filtered through a 200 μm inorganic membrane filter (Anotop 25, Whatman, Maidstone, UK) prior to membrane formation. Membranes with a thickness of 0.9 mm to 1.6 mm (in the hydrated state) were produced by casting at 180 °C from dimethyl sulfoxide (DMSO), and then converted to the H^+-form by boiling in 4 M H_2SO_4–methanol for 1 h, in methanol for 30 min, and in DI water for 30 min. To fabricate the IPMCs,[5] these solution-processed Nafion® surfaces were roughened by mechanically rubbing with 400-grain sandpaper to increase the surface area. Electroless plating of platinum was performed by following a multi-step procedure.[5] A platinum salt complex $[Pt(NH_3)_4]Cl_2$ (Aldrich) was used to make an aqueous solution with a concentration of 2 mg mL^{-1} solution. The H^+-form Nafion® membrane was allowed to equilibrate with the platinum salt solution overnight. After rinsing with DI water, the membrane was immersed in DI water and the Pt^{2+} ions in the membrane were reduced to Pt metal particles using 5% by weight aqueous sodium borohydride ($NaBH_4$, Aldrich). The addition of $NaBH_4$ was carried out in seven steps at 30 min intervals, over which the temperature was ramped from 40 °C to 60 °C. After completion of the initial series

of $NaBH_4$ additions, a final addition was carried out and reduction was allowed to proceed for 1.5 h. The electroded membrane was then removed and rinsed in DI water before immersion in 0.1 M HCl to convert the material to the acid form. The whole reduction process above was carried out for three cycles to produce the final IPMCs used in the current investigation. H^+-form IPMCs were further neutralized to contain tetramethylammonium (TMA^+) or sodium (Na^+) ions by soaking in excess (*ca.* 5×) aqueous solutions of the tetramethylammonium hydroxide (TMAOH, Aldrich) or sodium hydroxide (NaOH, Aldrich), respectively.

2.3 Neutron imaging

Direct imaging of an electrically induced water–counterion concentration gradient profile across the IPMC cross-section was acquired using a neutron imaging method available at the National Institute of Standards and Technology (NIST) Center for Neutron Research (NCNR).[28,30] At the NCNR, the neutron beam is processed through collimators, filters, an aperture, and an evacuated flight tube. Beam characteristics employed for the present experiment include the thermal neutron fluence rate of 1.9×10^9 cm^{-2} s^{-1} with L/D ratio of 1200 where L (6 m) is the distance between the source and the detector and D (5 mm) is the source aperture diameter. In terms of neutron detection schemes, a micro-channel plate (MCP)-based counting detector was employed. The MCPs doped with high efficiency neutron conversion materials, such as ^{10}B or ^{157}Gd, allow a high spatial resolution of 25 μm. The samples of IPMC prepared for neutron imaging were 2.0 cm in length, 0.5 cm in width and 0.9 mm to 1.6 mm in thickness (in the hydrated state). IPMC samples were equilibrated with DI water for 24 h before data acquisition. Hydrated IPMCs were then placed between copper electrodes sandwiched between Teflon spacers using the sample holder shown in Fig. 2, which inhibited the IPMC movement under electrical stimulation during the data acquisition.

2.4 Sample preparation for atomic force microscopy

H^+-form Nafion® was dissolved into a solvent system consisting of volume fractions of 50% ethanol and 50% DI water by heating the mixture to 250 °C in a pressure vessel for 2 h. The solution was filtered through a 200 μm inorganic membrane filter (Anotop 25, Whatman, Maidstone, UK) and deposited at room temperature onto the surface of a steel AFM stage puck to which a copper wire had been adhered using colloidal silver (Fig. 3). In order to minimize corrosion, exposure of the copper wire to the laboratory environment was minimized prior to imaging. The Nafion® film was formed by evaporating the solvent in a vacuum oven at a pressure of 33 kPa and a temperature of 50 °C.

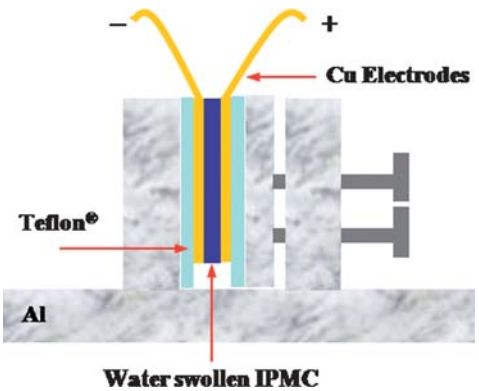

Fig. 2 Outline of the sample holder exposed in the neutron beam path.

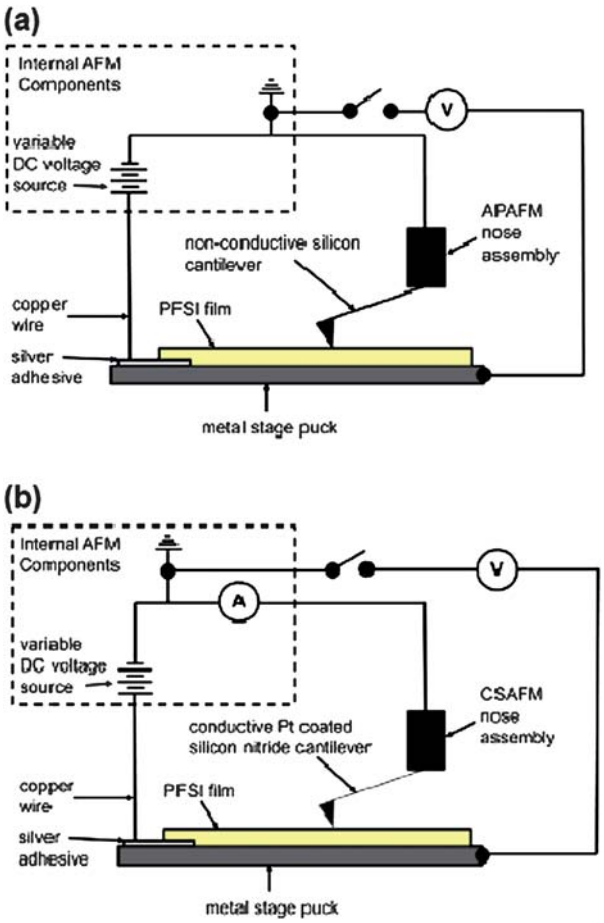

Fig. 3 Schematic drawings of (a) APAFM and (b) CSAFM. AFM voltage supply verified externally using multimeter. Non-conductive silicon cantilever in (a) acts as open switch. Conductive cantilever in (b) acts as closed switch.

2.5 Atomic force microscopy

AFM measurements were made in an environmental chamber at room temperature where the relative humidity (RH) was controlled by a nitrogen purge and kept between 60% and 70%. The morphology and response to an applied electrical field were studied using an Agilent 5500 AFM (Agilent Technologies, Santa Clara, CA) in both tapping mode atomic force microscopy with an applied potential (APAFM) and current sensing atomic force microscopy (CSAFM) modes. The AFM has a variable voltage source attached to the copper wire (Fig. 3) that is capable of applying a potential of −10 V to +10 V to the stage. APAFM was used to image both topography (height image) and domain behavior (phase image) of the cast films using a non-conductive silicon cantilever (RTESP, Veeco, Santa Barbara, CA) with a nominal resonant frequency of 300 kHz and a nominal force

constant of 40 N m^{-1}. A bias ranging from 0 V to +3 V was applied to the metal stage puck through the attached copper wire and the topography and phase images were taken as a function of applied voltage using the same type of non-conductive cantilever (Fig. 3a, applied potential). In APAFM a static electrical field is generated and there is no counter electrode. The changes in phase response of the cantilever are monitored with respect to voltage applied to the PFSI membrane. During APAFM, the ratio of the set point amplitude to the free amplitude (A/A_0) was maintained at a constant value.

CSAFM was used to probe the topography and local conductivity of the film with a bias ranging from −2 V to +2 V. A conductive platinum-coated silicon nitride cantilever (N9540-60002, Agilent Technologies, Santa Clara, CA) with a nominal force constant of 0.35 N m^{-1} was used for imaging (Fig. 3b). In CSAFM the conductive tip serves as the counter electrode. Current flows perpendicular to the PFSI membrane surface in the same direction and at similar voltages as the planar actuator. Topography and current images (detection of localized current) were obtained in contact mode. The voltage of the applied bias was verified by measuring the voltage between the metal stage puck and a ground on the AFM using a multimeter. During CSAFM the set point was maintained at a constant value. Data were processed using Gwyddion 2.10 software to improve image quality and remove artifacts. Images were leveled by mean plane subtraction, and scan lines were removed by matching the height median.

3. Results and discussion

Typical actuation performance of Nafion®-based IPMC undergoing deformation in response to an applied electrical potential is shown in Fig. 4. Overlaid in each captured image is a schema showing the position on the electrical square wave excitation, denoted by an X, at which the image was acquired. In the initial image, Fig. 4a, the IPMC is clamped vertically between copper electrodes prior to application of the electrical stimulus. Without any electrical stimulation, the water–counterion distribution is expected to remain uniform across the IPMC thickness. Fig. 4b shows the maximum bending of the IPMC immediately prior to the polarity switch of the applied square wave, while Fig. 4c shows the maximum bending in the opposite direction. Assuming a hydraulic mechanism, the electrical stimulation is expected to attract counterions along with water molecules toward the cathode (Fig. 4b), which should yield a water–counterion concentration gradient across the IPMC thickness. With a reversed polarity (Fig. 4c), counterions and water molecules are expected to travel to the other side of the IPMC, which will reverse the water–counterion concentration gradient.

3.1 Neutron imaging of hydrated IPMC element

Neutron radiography is an ideal tool to investigate the potential establishment of a water–counterion concentration gradient under electrical stimulation. Neutrons interact with materials differently than X-rays and hydrogen atoms have a uniquely high neutron scattering cross-section compared to other atoms including C, F, O, Na, S and Al (that are components of Nafion® and sample holders). Hydrogen atoms in the water molecules and the tetramethylammonium (TMA^+) counterions will yield a strong attenuation of the impingent neutron beam according to eqn (1):

$$I = I_0 \exp\left(-\sum_i \mu_i t_i\right) \quad (1)$$

where I represents the neutron intensity attenuated while passing through the specimen, I_0 is the incident neutron intensity, μ_i is referred to as the neutron attenuation coefficient of the material i, and t_i is the material thickness exposed in the beam path. By placing the working IPMC into the neutron beam path during electrical stimulation, it is possible to detect contrast variations in neutron transmission across the IPMC thickness with varying water–counterion concentrations. It is expected that any water–counterion concentration gradient created across the thickness of the Nafion® membrane will be detected as a neutron intensity gradient in the outgoing neutron beam. The raw imaging data were acquired before and after application of the electrical stimulus (3 V direct current, VDC) with an IPMC swollen with water and neutralized to contain TMA^+ counterions. The neutron imaging data acquired before any electrical stimulation were used as the reference (*i.e.*, with an equilibrium, isotropic water–counterion distribution across the film thickness). Fig. 5a shows one such processed image where all of the sample holder features and electrodes that do not change with electrical stimulation are normalized and not visible in the resulting image. In this image, water–counterion-depleted zones are represented by red color pixels, while water–counterion-rich zones are represented by blue color pixels. The sample thickness (*ca.* 950 μm) is represented by two vertical bars with a double-headed arrow and the direction of H_2O–TMA^+ migration indicated by a single-headed arrow. Fig. 5b shows a plot of the change in optical density (Δod) across the IPMC thickness. Δod is defined as $-\ln(I_{after}/I_{before})$ where I_{before} and I_{after} represent the intensities of neutron beam attenuated while passing through the IPMC

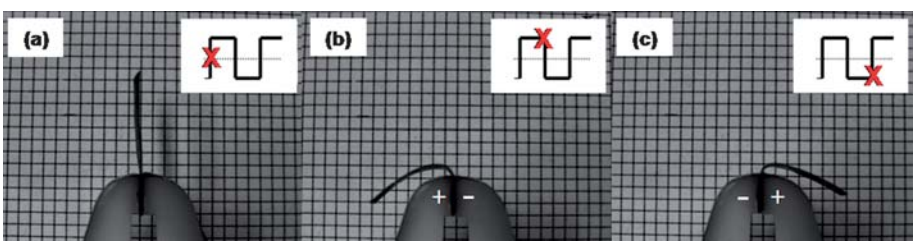

Fig. 4 IPMC actuation under applied electrical voltage: (a) 0 V, (b) +3 V, and (c) −3 V. Each image was captured at the position of X on the excitation square wave (square-grid dimensions of 2 mm).

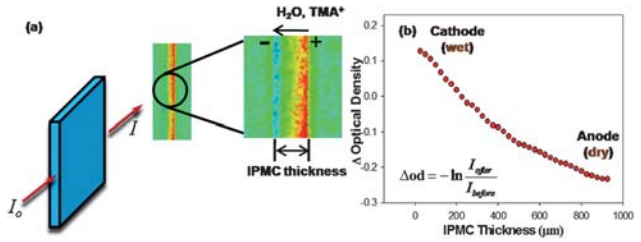

Fig. 5 (a) Colorized images showing water–tetramethylammonium (TMA^+)-depleted zones represented by red pixels and water–TMA^+-rich areas represented by blue pixels. IPMC was subjected to 3 VDC. (b) Water–counterion gradient profile across the IPMC thickness. Change in optical density (Δod) is defined as $-\ln(I_{after}/I_{before})$ where I_{after} and I_{before} represent the neutron intensities attenuated while passing through the IPMC sample before and after electrical stimulation, respectively.

sample before and after electrical stimulation, respectively. These data clearly demonstrate that a water–counterion concentration gradient profile is established with the application of an electric field across the IPMC thickness, indicating that water–counterion molecules are redistributing away from the anode side of the IPMC.

The gradient in Δod observed in Fig. 5 is attributed to both water and counterions due to the fact that water and TMA^+ both have an abundance of hydrogen atoms, in contrast to the perfluorinated ionomer matrix. To selectively characterize solvent migration, the IPMC is neutralized with Na^+ ions and swollen with H_2O. Because the H atom has almost 25 times larger scattering cross-section than the Na atom, the neutrons will only "see" the migration of H_2O, not Na^+, although both solvent and counterions are suggested to be redistributed under electrical stimulation in a hydraulic model.[6,22,23] Fig. 6 shows the time and space-resolved neutron attenuated raw intensity *versus* pixel location data along the H_2O swollen, Na^+-form IPMC cross-section. Fig. 6a compares data acquired at 0 s and 30 s under 3 V and also identifies the position of IPMC along with other components of the sample holder. It should be noticed that the water-swollen IPMC significantly attenuates the neutron beam compared to the Cu electrode and PTFE spacer, leading to the U shape profile observed in the raw data. As expected, no water concentration gradient is observed prior to electrical stimulation,

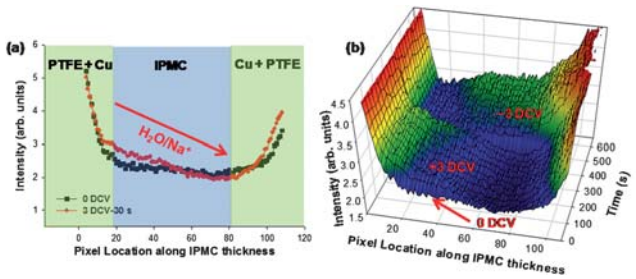

Fig. 6 Raw neutron intensity *versus* pixel location along H_2O swollen, Na^+-form IPMC cross-section placed between copper electrodes sandwiched between Teflon spacers. (a) Data taken at 0 s and 30 s under 3 V and (b) data acquired over 300 s before and after polarity reversal (1 pixel represents 25 μm). Since the flat field is not uniform, the raw data demonstrate a slight gradient even at 0 V.

which indicates uniform/random water distribution along the IPMC cross-section (*i.e.*, a nearly flat intensity profile across the IPMC). Electrical stimulation of 3 V for 30 s rapidly creates a distinct water concentration gradient (*i.e.*, a non-flat intensity profile sloping from the anode to the cathode) across the IPMC thickness.

Fig. 6b shows data acquired over 300 s before and after polarity reversal. The initially established water concentration gradient clearly remains over 300 s and the slope of this gradient is quickly inverted as soon as the polarity is switched, which explains the rapid macroscopic bending movement of IPMCs with polarity switching. Previous IPMC studies often observed the back-relaxation in strain and bending force under dc electrical stimulation.[20,32] While not specifically investigated in our initial study, this persistent gradient suggests that back-relaxation may be related to a segmental relaxation of the polymer matrix as opposed to a back-diffusion of water and/or ions.

To selectively characterize counterion redistribution during electrical stimulation, two sets of IPMC samples were prepared. One sample was neutralized with Na^+ ions while the other with TMA^+ ions. Both IPMC samples were then swollen with D_2O as opposed to H_2O. It should be pointed out that, in our controlled experiment with Nafion® 117-based IPMCs, no noticeable difference in actuation performance was observed upon solvent switching from H_2O to D_2O. However, the use of D_2O as opposed to H_2O will cause about a factor of 10 decrease in an effective solvent scattering cross-section (defined as the products of cross-section and concentration for each element) and thus the observed change in the neutron attenuation will be dominated by the counterions containing H atoms such as with TMA^+. Fig 7a and b show Δod profiles obtained for IPMC samples neutralized with Na^+ and TMA^+ ions, respectively. For each counterion, the IPMC was subjected to electrical stimulation of 3 V and the response of Δod was monitored for an extended time period, up to 20 min. As expected, for the Na^+-neutralized IPMC (Fig. 7a), the Δod profiles demonstrate a gradient that is about 10 times smaller than that in Fig. 6, consistent with the reduction in the scattering cross-sections. However, the Δod profiles for TMA^+-neutralized IPMC (Fig. 7b) clearly show that electrical stimulation yields a distinct counterion concentration gradient. Thus, this experiment demonstrates that the mobile ions in IPMCs are redistributed across the IPMC thickness along with water molecules in response to the applied electric field.

In Fig. 5b and 7b, the positive Δod near the cathode indicates an increased concentration of water and counterions under electrical stimulation compared to that observed without

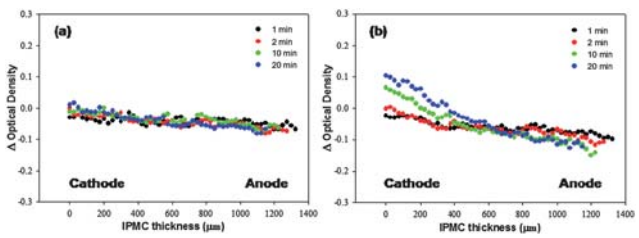

Fig. 7 Change in optical density (Δod) profiles across D_2O swollen IPMCs neutralized to contain (a) Na^+ and (b) TMA^+ ions. IPMCs were electrically stimulated by 3 V for an extended time period.

application of an electric field. On the contrary, the negative Δod near the anode indicates a decreased concentration of water and counterions under electrical stimulation compared to the uniform distribution in the absence of an applied field. This is indeed the first direct evidence of water and counterion redistribution during electrical stimulation in these new stimuli-responsive materials, and evidently indicates that the hydraulic phenomenon is a strong contribution to the overall actuation mechanism. It should also be pointed out that the Δod profiles shown in Fig. 5b and 7b display a uniform gradient across the film as opposed to a step-like profile near the electrode layers. Thus, a more accurate description of this proposed hydraulic mechanism should involve the entire IPMC thickness, as opposed to simply a creation of cation-rich and cation-poor boundary layers near the electrode–membrane interfacial regions.

3.2 AFM on PFSI films under electrical stimulation

The IPMC actuation mechanism was further characterized by atomic force microscopy. Various AFM studies on PFSIs have been performed previously with the goal of identifying the size and shape of hydrophilic domains distributed within the hydrophobic PTFE matrix.[33–35] More recent efforts have involved the use of a platinum-coated conductive AFM tip to determine the distribution of electrochemically active ionic domains.[36,37] However, there has been no detailed investigation regarding surface characteristics of PFSIs that are under the influence of electrical stimulation, which is clearly needed to understand the mechanistic details of IPMC actuation. This work describes the use of a combination of APAFM and CSAFM to capture surface morphological response and local conductivities, respectively, as a function of an applied electric field.

Ion and water redistribution under electrical stimulation was probed by measuring the local mechanical energy dissipation on the surface of a PFSI membrane subjected to an applied bias voltage using APAFM (Fig. 8). In APAFM the cantilever was operated in the intermittent contact regime to minimize destructive lateral forces on the sample surface while both topographical and phase images were obtained. By measuring the phase shift with constant excitation force, differences in probe–tip sample interactions produce compositional contrast in a heterogeneous sample.[38] Contrast arises from differences in mechanical energy dissipation between the tip and the sample.[39,40] In the intermittent contact regime, softer, more viscous, energy dissipative components appear as darker features in the phase image, while harder, more elastic, components appear brighter.[41] In Fig. 8 topographical images are presented on the left, and the corresponding phase images are on the right. In Fig. 8a and b, there is no applied bias voltage. In Fig. 8c and d, a 1 V bias was applied to the stage puck producing a negative charge on the puck surface in contact with the PFSI membrane. No significant change in surface roughness is observed when a 1 V bias is applied, but the average phase shift of the cantilever's response to the surface increases from 14.3° to 23.3°, indicating an overall decrease in energy dissipation. The same trend is observed in Fig. 8f and h as the bias is increased from 1 V to 3 V. At 3 V, the average phase shift of the cantilever increases

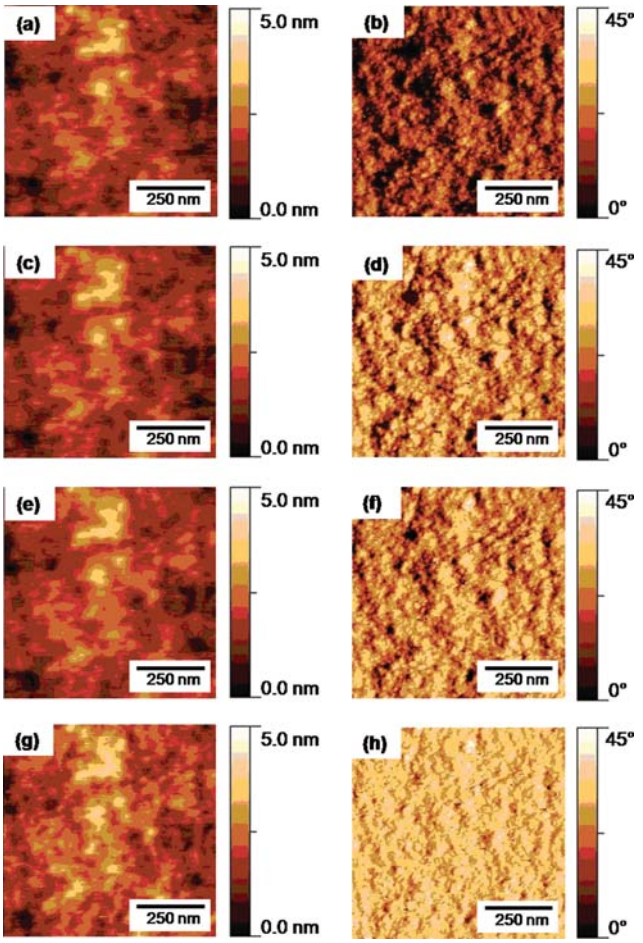

Fig. 8 APAFM topographical (left) and corresponding phase (right) images of PFSI film as a function of applied bias voltage: (a and b) 0 V, (c and d) 1 V, (e and f) 2 V, (g and h) 3 V.

to 30.1°. Surface roughness and average phase shift data are summarized in Table 1 below. Table 1 shows that the surface roughness remains relatively constant, while the phase shift increases with applied voltage. The disappearance of the darker, more energy dissipative features as the applied bias is increased indicates that the total surface has become more energy conservative. Since the presence of water on the surface of a membrane will increase the energy dissipative characteristics of the surface, the observed increase in energy conservation of the PFSI membrane surface suggests that the surface is becoming dehydrated. This observation is in complete agreement with the neutron imaging results above and further supports the mechanism of proton and water migration to the negatively charged substrate as shown in the schematic presented in Fig. 10b.

Table 1 Summary of surface roughness and phase shift as a function of applied voltage

	Topographical roughness/nm	Phase average shift/°
0 V	0.57	14.3
1 V	0.57	23.3
2 V	0.57	23.9
3 V	0.60	30.1

Further examination of the electrically stimulated gradients was conducted using the CSAFM method (operating in the contact regime) and presented in Fig. 9 with topographical images on the left, and the corresponding current images on the right (note that the scan size is larger than that in Fig. 8). In Fig. 9a (topography) and b (current), a +2 V bias was applied to the metal stage puck giving the substrate surface of the PFSI membrane a negative charge. The conductive domains (brighter areas, see scale bar) in Fig. 9b correspond to the high regions of the topographical image in Fig. 9a. Current flow is isolated to the bright areas that indicate measurable current. The average current calculated from every point measured across the surface of Fig. 9b is 2.8 pA. It should be pointed out that the image scale in Fig. 9b is reduced to increase contrast. In Fig. 9c (topography) and d (current), the polarity is now reversed and −2 V bias is applied to the substrate, yielding a positive charge at the substrate surface of the sample. The average current of Fig. 9d is −90.6 pA, which suggests that conduction occurs over the entire surface. The regions of high current flow in this image are the dark features, and correspond to the dark, lower regions of the topography image (see scale bar). Average diameter of the conductive domains determined by image analysis is 41 nm with a standard deviation of 8 nm. The inset in Fig. 9d shows a step change in voltage from −2 V (bottom of inserted image) to +2 V (top of inserted image) during a single scan. While little quantitative information can be obtained from the inset due to the time dependent dynamic processes that occur from a sudden change in applied bias, it qualitatively shows the shift in surface conductivity of the PFSI membrane as the substrate bias is changed. The inset shows that a negative charge applied to the substrate produces a negative charge on the top surface of the PFSI membrane, and a positive charge applied to the substrate produces a positive charge on the PFSI membrane surface. This further illustrates the change in PFSI membrane response as a function of applied voltage.

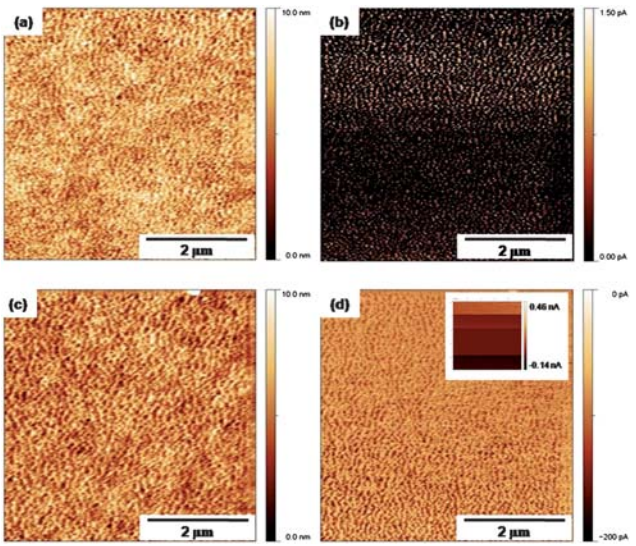

Fig. 9 CSAFM topographical (left) and current (right) images of PFSI film: (a and b) +2 V, (c and d) −2 V. Each current image is composed of 512 × 512 individual data points. The inset in (d) shows the response of the surface of the PFSI membrane as a step change in voltage is applied to the substrate from −2 V (bottom of image) to +2 V (top of image).

The PFSI investigated in this study is known to form a phase-separated morphology where the ionic domains, termed ionic clusters, are distributed throughout the non-polar polytetrafluoroethylene (PTFE) matrix, and continuous ionic channel formation in a hydrated condition provides the percolation pathway for ionic conduction.[11,42] When no charge is applied to

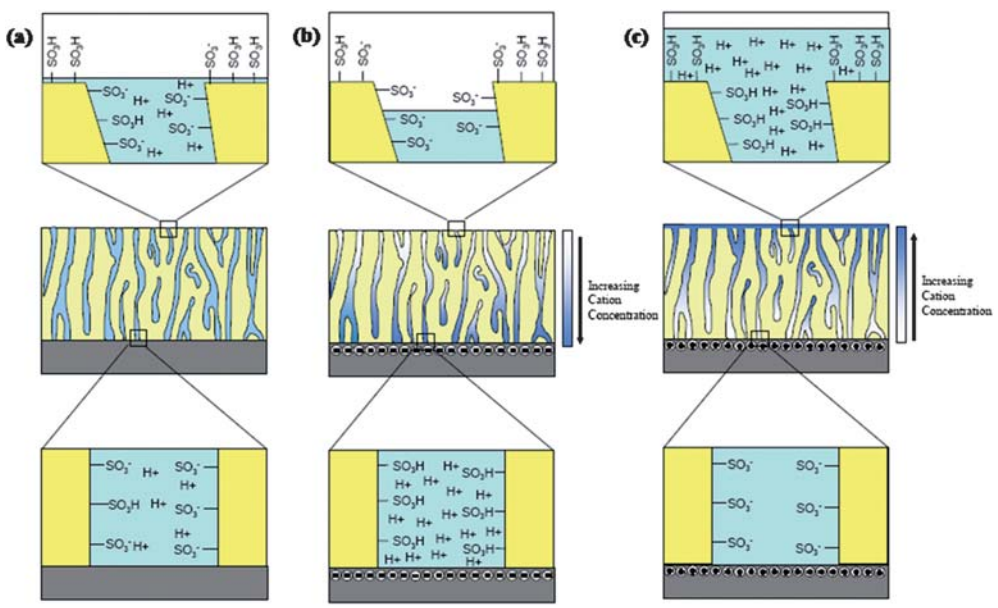

Fig. 10 (a) Illustration of the equilibrium state between sulfonate groups and protons in the PFSI membrane with no applied bias, (b) illustration of proton and water migration to the negatively charged substrate and formation of isolated sulfonate-rich domains and dehydration on the top surface of the PFSI membrane, and (c) illustration of proton and water migration away from the positively charged substrate forming a cationic film on the top surface of the PFSI membrane and neutralization of the positively charged substrate by non-mobile sulfonate ions.

the membrane, the sulfonate groups residing in the interfacial region between the PTFE matrix and the ionic channel are in equilibrium with protons in solution, and the sulfonate groups residing on the top surface of the PFSI membrane are in equilibrium with protons residing in the thin liquid layer present on the top surface of the PFSI membrane. This is illustrated schematically in Fig. 10a.

The light features in Fig. 9b correspond to the dark features in Fig. 9a and indicate that these are actively conductive channels. The direction of positive current flow in Fig. 9b suggests that the light features represent the immobile, negatively charged sulfonate groups producing positive current flow to the grounded, platinum-coated cantilever. The dark, continuous region of Fig. 9b corresponds to the light continuous region of Fig. 9a, suggesting that this is the non-conductive PTFE matrix. The direction of current flow indicates that the surface is absent of positively charged cations and suggests that these species have migrated to the negatively charged substrate as shown in the schematic presented in Fig. 10b.

In Fig. 9d the darker features correspond to the dark features in Fig. 9c, providing further evidence that these domains represent the actively conductive channels. The direction of negative current flow in Fig. 9d suggests that the mobile protons and water have migrated to the surface giving it a positive charge. The magnitude of the negative current flow and the presence of current flow over the entire surface suggest that the cationic fluid has not only migrated to the surface of the actively conducting domains but also has actually formed a cationic film on the top surface of the PFSI membrane, which is illustrated schematically in Fig. 10c.

4. Conclusions

We employed two different techniques, neutron imaging and atomic force microscopy, in an effort to fundamentally characterize electrically stimulated water–counterion redistribution which has been suggested to be an important consideration in the IPMC actuation mechanism. While the neutron imaging method provided a bulk characterization (cross-sectional analysis) of water–counterion migration across the IPMC thickness, AFM allowed surface characterization of the nanoscale morphology and local surface properties due to migration of water–counterion under electrical stimulation. The time and space-resolved neutron imaging experiment showed that water gradients were established along the IPMC cross-section during 30 s under 3 VDC stimulation. With a sudden switch in polarity, the gradient reversed rapidly, in agreement with the rapid actuation response typically observed with IPMCs. Moreover, under this dc stimulation, the water gradient was observed to persist over an extended time period (300 s). While not specifically probed in this initial investigation, this persistent gradient suggests that the often observed back-relaxation in strain and bending force of dc stimulated IPMCs may be related to a segmental relaxation of the polymer matrix as opposed to a back-diffusion of water and/or ions. IPMCs neutralized with TMA^+ ions and swollen with D_2O were used to directly probe counterion redistribution under electrical stimulation. Under 3 V, a distinct sloping in the optical density profile was observed. A positive sign of optical density near the cathode indicated that counterions were attracted toward the negatively charged electrode.

Water–counterion migration in response to various voltages was characterized using APAFM. The increase in energy conservation of the PFSI membrane surface suggested that the surface was being dehydrated due to migration of protons and water to the negatively charged substrate, which correlates very well with the neutron imaging results. Water–counterion migration was further supported by CSAFM. Under a +2 V bias, only a low 2.8 pA of average current was detected over the PFSI surface. This indicated that positively charged cations were essentially absent on the surface. On the contrary, application of −2 V bias to the substrate–sample interface led to a high average current of −90.6 pA on the opposing surface, which suggests that the protons and water have migrated to the surface away from the positively charged substrate.

While the true mechanism of actuation in IPMCs has remained under debate, the direct evidence in this study has demonstrated for the first time that the actuation response involves a strong hydraulic contribution. With an electrical field established between the IPMC electrode layers, mobile cations and their water molecules of hydration rapidly migrate to the cathode (negative electrode). This electrically stimulated gradient in water concentration across the ionic polymer membrane creates opposing swelling (cathode side) and deswelling (anode side) pressures that induce a bending of the actuator toward the anode. With a switch in polarity, the water and ions move rapidly across the ionic polymer film to establish a reverse gradient that yields a subsequent reversal in the IPMC curvature.

Notes and references

1 A. J. Duncan, D. J. Leo and T. E. Long, *Macromolecules*, 2008, **41**, 7765.
2 J. K. Park and R. B. Moore, *ACS Appl. Mater. Interfaces*, 2009, **1**, 697.
3 A. K. Phillips and R. B. Moore, *Polymer*, 2005, **46**, 7788.
4 M. Shahinpoor, *Electrochim. Acta*, 2003, **48**, 2343.
5 M. Shahinpoor and K. J. Kim, *Smart Mater. Struct.*, 2001, **10**, 819.
6 M. Shahinpoor, Y. Bar-Cohen, J. O. Simpson and J. Smith, *Smart Mater. Struct.*, 1998, **7**, R15.
7 M. Shahinpoor, *Smart Mater. Struct.*, 1992, **1**, 91.
8 K. Sadeghipour, R. Salomon and S. Neogi, *Smart Mater. Struct.*, 1992, **1**, 172.
9 K. Asaka, K. Oguro, Y. Nishimura and M. Mizuhata, *Polym. J. (Tokyo)*, 1995, **27**, 436.
10 Certain trade names and company products are mentioned in the text or identified in an illustration in order to adequately specify the experimental procedure and equipment used. In no case does such identification imply recommendation or endorsement by the National Institute of Standards and Technology, nor does it imply that the products are necessarily the best available for the purpose.
11 K. A. Mauritz and R. B. Moore, *Chem. Rev.*, 2004, **104**, 4535.
12 K. Schmidt-Rohr and Q. Chen, *Nat. Mater.*, 2008, **7**, 75.
13 M.-H. Kim, C. J. Glinka, S. A. Grot and W. G. Grot, *Macromolecules*, 2006, **39**, 4775.
14 L. Rubatat, A. L. Rollet, G. Gebel and O. Diat, *Macromolecules*, 2002, **35**, 4050.
15 M. D. Bennett and D. J. Leo, *Sens. Actuators, A*, 2004, **115**, 79.
16 M. D. Bennett and D. J. Leo, *Smart Mater. Struct.*, 2003, **12**, 424.
17 M. Shahinpoor and K. J. Kim, *Smart Mater. Struct.*, 2000, **9**, 543.
18 K. Onishi, S. Sewa, K. Asaka, N. Fujiwara and K. Oguro, *Electrochim. Acta*, 2001, **46**, 1233.
19 S. Nemat-Nasser and Y. Wu, *J. Appl. Phys.*, 2003, **93**, 5255.
20 S. Nemat-Nasser and Y. Wu, *Smart Mater. Struct.*, 2006, **15**, 909.

21 V. K. Nguyen, J. W. Lee and Y. Yoo, *Sens. Actuators, B*, 2007, **120**, 529.
22 P. G. De Gennes, K. Okumura, M. Shahinpoor and K. J. Kim, *Europhys. Lett.*, 2000, **50**, 513.
23 M. Shahinpoor, *Smart Mater. Struct.*, 1994, **3**, 367.
24 L. M. Weiland and D. J. Leo, *Smart Mater. Struct.*, 2004, **13**, 323.
25 S. Nemat-Nasser and J. Y. Li, *J. Appl. Phys.*, 2000, **87**, 3321.
26 L. Naji, J. A. Chudek and R. T. Baker, *Soft Matter*, 2008, **4**, 1879.
27 L. Naji, J. A. Chudek and R. T. Baker, *J. Phys. Chem. B*, 2008, **112**, 9761.
28 R. J. Bellows, M. Y. Lin, M. Arif, A. K. Thompson and D. Jacobson, *J. Electrochem. Soc.*, 1999, **146**, 1099.
29 M. A. Hickner, N. P. Siegel, K. S. Chen, D. N. McBrayer, D. S. Hussey, D. L. Jacobson and M. Arif, *J. Electrochem. Soc.*, 2006, **153**, A902.
30 R. Satija, D. L. Jacobson, M. Arif and S. A. Werner, *J. Power Sources*, 2004, **129**, 238.
31 R. B. Moore and C. R. Martin, *Anal. Chem.*, 1986, **58**, 2569.
32 J. Lu, S.-G. Kim, S. Lee and I.-K. Oh, *Adv. Funct. Mater.*, 2008, **18**, 1290.
33 A. M. Affoune, A. Yamada and M. Umeda, *J. Power Sources*, 2005, **148**, 9.
34 A. Lehmani, S. Durand-Vidal and P. Turq, *J. Appl. Polym. Sci.*, 1998, **68**, 503.
35 R. S. McLean, M. Doyle and B. B. Sauer, *Macromolecules*, 2000, **33**, 6541.
36 X. Xie, O. Kwon, D. Zhu, T. V. Nguyen and G. Lin, *J. Phys. Chem. B*, 2007, **111**, 6134.
37 D. A. Bussian, J. R. O'Dea, H. Metiu and S. K. Buratto, *Nano Lett.*, 2007, **7**, 227.
38 J. Tamayo and R. Garca, *Langmuir*, 1996, **12**, 4430.
39 J. Tamayo and R. Garcia, *Appl. Phys. Lett.*, 1997, **71**, 2394.
40 J. Tamayo and R. Garcia, *Appl. Phys. Lett.*, 1998, **73**, 2926.
41 P. J. James, M. Antognozzi, J. Tamayo, J. McMaster, J. M. Newton and M. J. Miles, *Langmuir*, 2001, **17**, 349.
42 T. D. Gierke, G. E. Munn and F. C. Wilson, *J. Polym. Sci., Polym. Phys. Ed.*, 1981, **19**, 1687.

